

This discussion paper is/has been under review for the journal Atmospheric Chemistry and Physics (ACP). Please refer to the corresponding final paper in ACP if available.

Environmental controls on pyrocumulus and pyrocumulonimbus initiation and development

N. P. Lareau and C. B. Clements

Fire Weather Research Laboratory, San José State University, San José, California, USA

Received: 21 September 2015 – Accepted: 14 October 2015 – Published: 27 October 2015

Correspondence to: N. P. Lareau (neil.lareau@sjsu.edu)

Published by Copernicus Publications on behalf of the European Geosciences Union.

Pyrocumulus and pyrocumulonimbus initiation and development

N. P. Lareau and
C. B. Clements

Title Page

Abstract

Introduction

Conclusions

References

Tables

Figures

◀

▶

◀

▶

Back

Close

Full Screen / Esc

Printer-friendly Version

Interactive Discussion

Abstract

In this paper we present the first direct observational evidence that the condensation level in pyrocumulus and pyrocumulonimbus clouds can significantly exceed the ambient lifted condensation level. In addition, we show that the environmental thermodynamic profile, day-to-day variations in humidity, and ambient wind shear all exert significant influence over the onset and development of pyroconvective clouds. These findings are established using a scanning Doppler lidar and mobile radiosonde system during two large wildfires in Northern California, the Bald and Rocky Fires. The lidar is used to distinguish liquid water from smoke backscatter during the plume rise, and thus provides a direct detection of plume condensations levels. Plume tops are subsequently determined from both the lidar and nearby radar observations. The radiosonde data, obtained adjacent to the fires, contextualizes the lidar and radar observations, and enables estimates of the plume ascent, convective available potential energy, and equilibrium level. A note worthy finding is that in these cases the Convective Condensation Level, not the Lifted Condensation Level, provides the best estimate of the pyrocumulus initiation height.

1 Introduction

Pyrocumulus (pyroCu) form when wildfire convective plumes rise to their condensation level and subsequently develop cumuliform cloud tops (American Meteorological Society, 2012a). The extent of pyroCu development depends on the relationships amongst atmospheric stratification, ambient moisture, and fire fluxes of heat and moisture (Potter, 2005; Luderer et al., 2006, 2009; Frietas et al., 2007). Non-developing pyroCu are relatively innocuous, whereas developing pyroCu release moist instability aloft and thereby trigger deep convective clouds that sometimes grow into pyrocumulonimbus (pyroCb). Compared to their lesser counterparts, pyroCb possess glaciated cloud tops and can thus generate precipitation, downdrafts, and lightning (American Meteorolog-

Pyrocumulus and pyrocumulonimbus initiation and development

N. P. Lareau and
C. B. Clements

Title Page

Abstract

Introduction

Conclusions

References

Tables

Figures



Back

Close

Full Screen / Esc

Printer-friendly Version

Interactive Discussion



Pyrocumulus and pyrocumulonimbus initiation and development

N. P. Lareau and
C. B. Clements

Title Page

Abstract

Introduction

Conclusions

References

Tables

Figures

◀

▶

◀

▶

Back

Close

Full Screen / Esc

Printer-friendly Version

Interactive Discussion



A limitation of this study is the anecdotal treatment of condensation levels, which are estimated, and the use of radiosonde observations that may not reflect the near fire environment.

In contrast to Potter (2005), Luderer et al. (2006, 2009) use high-resolution simulations and theoretical sensitivity calculations to conclude that “the combined effect of released moisture and heat from the fire almost always results in a higher cloud base compared to ambient conditions.” They also find that moisture released in combustion constitutes less than 10% of the pyroCu/Cb water budget with the remainder of the plume water resulting from entrained environmental air. While these modeled results are rather convincing, they lack clear observational support.

To that end, the only field observations that address plume moisture are from small scale grass fire experiments, where significant increases in water vapor mixing ratio are documented near the surface, but then decrease rapidly with height (Clements et al., 2006, 2007; Kiefer et al., 2012). While these observations are consistent with the dominant role of entrainment, such small-scale plumes may not be representative of deep convective plumes that extend into the upper troposphere or even lower stratosphere.

In this paper we present the first direct observations of condensation levels in two wildfire pyroCu/Cb cases. The fires, the Bald Fire and the Rocky Fire, were located in Northern California, and observations were conducted on 2 August 2014 and 30 July 2015, respectively. The pyroCu cloud bases and plume rise dynamics were measured using a mobile atmospheric profiling system (Clements and Oliphant, 2014) that included a scanning Doppler lidar and an upper-air radiosonde system which provided thermodynamic profiles immediately upstream of the fire perimeters. From these data, our results clearly show that observed plume condensation levels are substantially higher than the ambient LCL. Additional aspects of the plume rise, including limiting factors on convective growth and the role of environmental moisture are also examined.

2 The Bald Fire

The Bald Fire was started by lightning 31 July 2014 and subsequently developed a deep convective plume capped with pyroCu and then pyroCb on the afternoon of 2 August. Shortly after the pyroCu initiation ($\sim 14:00$ PDT) the afternoon MODIS overpass recorded a detailed image of the growing pyroCu, along with instantaneous observations of fire radiative power (FRP, Fig. 1a). The maximum FRP within the Bald Fire perimeter was 2645 MW, though the pyroCu, which interrupts the FRP computation, obscured much of the actively burning region.

2.1 Lidar observations

The truck-mounted Doppler lidar was situated ~ 7 km southwest of the fire where it conducted vertical sector scans of the windward edge of the developing smoke plume and pyrocumulus cloud. Figure 1b provides photograph from the lidar vantage point showing the towering smoke column capped with pyroCu/Cb, and at times pileus clouds. The lidar scans from this location provide a detailed picture of the plume edge and aspects of the plume rise, including the condensation level.

Figure 2, for example, shows a sequence of lidar scans during the plume rise spanning the 5 min period prior to the MODIS overpass. These data are expressed as the logarithmic attenuated backscatter coefficient (hereafter backscatter) in units of $\text{m}^{-1} \text{sr}^{-1}$. The backscatter is sensitive to micron-sized aerosol including smoke particles and liquid water droplets, and while the lidar beam ultimately attenuates in both, its attenuation is more rapid into cloud droplets. In addition, the signal-to-noise ratio (SNR) for cloud returns tends to be very high (> 1.2), whereas it is somewhat lower in smoke and other aerosol. These aspects of the data make direct detection of the condensation level within the plume possible. Banta et al. (1992), for example, determined pyrocumulus boundaries using a subjective identification from lidar backscatter patterns, and more broadly, terrestrial lidars are regularly used to determine cloud base heights (e.g., Hogan et al., 2003)

Pyrocumulus and pyrocumulonimbus initiation and development

N. P. Lareau and
C. B. Clements

Title Page

Abstract

Introduction

Conclusions

References

Tables

Figures

◀

▶

◀

▶

Back

Close

Full Screen / Esc

Printer-friendly Version

Interactive Discussion

In the present case, condensation is first apparent within the developing convective column at ~ 5500 m a.m.s.l. (all heights are a.m.s.l., above mean sea level, and hereafter just listed in meters), starting between 14:19 and 14:20 PDT (Fig. 2a, b). The cloud edge is marked by a distinct increase in the backscatter and more rapid attenuation giving the data a “crisper” edge that defines the pyroCu boundary. The nascent pyroCu then rapidly expands during the subsequent scans, obtaining a height of at least 8500 m by 14:24 PDT (Fig. 2e). The lidar range (9.6 km) limited the plume top detection, and as we show below the actual plume top was as high as 12 km.

The scans, which were roughly parallel to the mean wind direction, also reveal that the plume experienced significant variations in tilt with time, alternating between windward (Fig. 2a) and rearward sloping geometries (Fig. 2e). In fact, the windward protrusion of the plume was as much as 2 km away from its base. Large coherent eddies, or “ring vortices,” are also apparent along the plume edge, with inward clefts corresponding to enhanced flow into the plume (e.g., entrainment) and outward lobes reflecting flow towards the lidar (radial velocity data not shown).

Following the initial plume rise, sustained pyroCu were observed until 15:30 PDT, at which point the lidar was relocated for safety reasons. To aggregate the lidar scans during this period, Fig. 3a presents the time-maximum backscatter as a function of height and distance, and in Fig. 3b as a function of height only. These data reinforce many of the aspects of the initial plume rise sequence discussed above. For example, the plume went through many variations in “uprightedness”, manifest as an envelope of plume edge detections (Fig. 3a). It is also readily apparent from these data that there is a persistent transition in backscatter near 5500 m (green line in Fig. 3a, b). Below this level, the backscatter approximately linearly decreases with height, consistent with the turbulent entrainment of clear air into an aerosol-laden plume. In contrast, at 5500 m the backscatter sharply increases (as does the SNR, not shown), corresponding to the condensation level and development of the pyroCu. The backscatter intensity remains high there and above due to the continued presence of liquid water. Notably, the con-

result includes a surface-based stable layer that is not representative of daytime conditions. To address this shortcoming, the afternoon temperature (measured on the truck weather station) was used to infer the CBL depth using the “parcel method” (Holtzworth, 1964).

The adjusted sounding shows that the afternoon CBL extends from the surface (1364 m) to ~ 4000 m and is capped by a pronounced stable layer. Within the CBL, the water vapor mixing ratio is roughly constant at $\sim 5 \text{ g kg}^{-1}$, whereas above the CBL a layer of very dry air is observed with a water vapor mixing ratio of only $\sim 0.5 \text{ g kg}^{-1}$. Further aloft, near 400 hPa, a layer of higher humidity air, reflecting monsoonal moisture, is found. The height of the tropopause is ~ 13 km.

Relative to the observed profile, the “in cloud” profile is estimated by pseudo-adiabatically lifting a parcel from the lidar observed condensation level at 5500 m. The resulting parcel possesses 910 J kg^{-1} of convective available potential energy (CAPE), which is an upper bound on the energy available for buoyant ascent. The equilibrium level (EL) of the pyroCu parcel is 11 742 m, which is in close agreement with the radar estimated echo tops, but does not account for the inertial overshoot of the parcel, which is likely reflected in the localized region of radar plume heights exceeding 12 km (Fig. 4).

Also of note, the homogeneous freezing level (-38°C) in the plume profile occurs at 10 158 m and the temperature at the EL is -52°C , indicating that the upper portion of the cloud must be glaciated. As such, this particular pyroconvective cloud should be classified as a pyroCb. In fact, pyroCb from other nearby fires on that day were known to produce lightning as well as a significant and destructive fire-whirl (Muller and Herbster, 2014).

Lifted parcels

One of the main goals of this paper is to compare the observed plume properties with conventional estimates of condensational level and convective potential. To that end, in

Pyrocumulus and pyrocumulonimbus initiation and development

N. P. Lareau and
C. B. Clements

Title Page

Abstract

Introduction

Conclusions

References

Tables

Figures

◀

▶

◀

▶

Back

Close

Full Screen / Esc

Printer-friendly Version

Interactive Discussion



this subsection we consider three potential parcels as representations of the observed plume, each of which is shown in Fig. 5b.

Most unstable parcel: Each parcel in the ambient profile is lifted, first dry adiabatically, and then, if it saturates, along a moist adiabat. The “most unstable” (MU) parcel is identified as the parcel with the highest CAPE. In this case, the MU parcel originates in the CBL and produces an LCL of 4367 m, which is more than 1 km lower than the observed 5500 m condensation level. In addition, compared to the observed plume structure, the MU parcel possesses minimal CAPE and must overcome appreciable convective inhibition (CIN) before reaching its level of free convection.

Mixed layer parcel: Using the mean quantities of the lowest 100 hPa of the sounding a mixed layer (ML) parcel is lifted. This parcel encounters its LCL at 4641 m, possesses almost no CAPE, and also must overcome appreciable CIN. The LCL for the ML parcel exceeds that of the MU parcel because the layer averaged mixing ratio is less than the maximum mixing ratio in the CBL.

Convective Parcel: The convective condensation level (CCL) is the height at which the environment temperature profile supports saturation for the observed near-surface mixing ratio. In this case the mixing ratio is 5.2 g kg^{-1} and the corresponding CCL is found at 5549 m, which is very close to the observed condensation level of 5500 m. Commensurately, the EL and CAPE for the convective parcel are also close to the observed values. The convective temperature, which is the surface temperature that must be reached to support convection, is 36.4°C . The high temperature for the day was $\sim 29^\circ\text{C}$, making surface based convection extremely unlikely outside of the fire modified environment.

From these analyses it is clear that the plume condensation level is substantively higher than the ambient LCL, supporting the results of Luderer et al. (2006, 2009). Further, using the CCL, not the LCL, and assuming that the fire readily exceeds the convective temperature, provides the best representation of the plume condensation level in this case. This is a potentially useful diagnostic for forecasters and fire managers. It should be noted, however that the convective temperature and the associated

Pyrocumulus and pyrocumulonimbus initiation and development

N. P. Lareau and
C. B. Clements

Title Page	
Abstract	Introduction
Conclusions	References
Tables	Figures
◀	▶
◀	▶
Back	Close
Full Screen / Esc	
Printer-friendly Version	
Interactive Discussion	



adiabat up to the CCL do not necessarily reflect the actual properties of the lower plume. Rather, the plume must be superadiabatic near its base, cooling largely due to entrainment as it decays towards adiabatic ascent further aloft (Emanuel, 1994; Trentmann et al., 2006; Frietas et al., 2007).

3 The Rocky Fire

In this section we explore the impact of limiting processes on pyroCu development during the Rocky Fire. The Rocky Fire started on 29 July 2015 (cause unknown) in the coastal range of northern California and burned in complex terrain through fuels consisting of grass, brush, and conifers. Compared to the long-lived Bald Fire pyroCb, the Rocky Fire plumes were less vertically developed and more transient, persisting only for a few 10 s of minutes before dissipating.

3.1 Lidar observations

PyroCu were first observed starting at 15:55 PDT rising from the active northwest flank of the fire. Figure 6 shows a sequence of photographs (top panels) and contemporaneous lidar scans (bottom panels) detailing the onset and expansion of the cloud topped plume. The plume was initially observed as it penetrated through a stable layer at the top of the CBL, evident as a lateral smoke layer at ~ 2600 m in the backscatter data and as a diffuse haze in the photographs. During this time a thin pileus cloud accompanied the developing pyroCu and the lidar cloud returns were limited to a few points near the plume top (Fig. 6f).

By 16:03 PDT, however, a distinct cumuliform cloud had developed (Fig. 6b) and the lidar backscatter showed a commensurate increase in intensity and attenuation along the pyroCu edge (Fig. 6g). Based on these data the cloud base was at ~ 4200 m. The subsequent scans show the rapid pyroCu development, and by 16:09 PDT cloud edges

Pyrocumulus and pyrocumulonimbus initiation and development

N. P. Lareau and
C. B. Clements

Title Page

Abstract

Introduction

Conclusions

References

Tables

Figures

◀

▶

◀

▶

Back

Close

Full Screen / Esc

Printer-friendly Version

Interactive Discussion



were detected as high as 7500 m. Interestingly, soon thereafter the pyroCu detrained from the convective column and dissipated (not shown).

A second pyroCu growth event was observed starting at ~ 18:00 PDT (Fig. 7). This plume initiated ~ 2.5 km southeast of the lidar location allowing for a more detailed sampling of the plume base, including Doppler radial velocities. As in the previous case, the rapidly growing plume was first recorded as it rose through the boundary layer top, now at ~ 2300 m, and expanded into the free troposphere (Fig. 7a, e). Subsequent scans revealed the onset of pyroCu with a condensation level of ~ 4200 m, which is unchanged from the earlier Rocky Fire pyroCu event. In this case, however, the cloud top was not as well documented because attenuation at the cloud base shielded the lidar view of the upper plume.

An additional aspect of the observed plume rise is the tilt of the convective column, which varies during the pyroCu development. For example, the plume is at first more upright, and then becomes increasingly tilted within the boundary layer (compare Fig. 7e, i). The relationship between plume tilt, updraft strength, and ambient wind shear is elucidated in Figs. 8 and 9, which display vertical profiles of the horizontal wind and the lidar radial velocity during the plume rise, respectively.

The wind profiles exhibit significant wind shear, with strong (5–7 m s⁻¹) northwesterly winds near the surface transitioning to weak flow at the boundary layer top (0–1 m s⁻¹), then reversing to easterly flow aloft (Fig. 8). The observed near-surface wind speed maximum is atypical in the atmospheric boundary layer, and may reflect an inflow jet being drawn into the base of the plume.

Compared to the ambient winds, the radial velocities measured within the plume are large, with peak values in excess of 12 m s⁻¹ (Fig. 9). In fact, assuming that the flow within the plume is parallel to the plume centerline, which is semi-objectively determined for each scan, the maximum updraft strength is estimated to be in excess of ~ 18 m s⁻¹ at 18:08 PDT. Thereafter, the updraft strength diminishes and the plume becomes increasingly laid over. For example, the plume is initially inclined at ~ 60 degrees from the horizontal (Fig. 9a), but just 5 min later is inclined at only 45 degrees

Pyrocumulus and pyrocumulonimbus initiation and development

N. P. Lareau and
C. B. Clements

Title Page

Abstract

Introduction

Conclusions

References

Tables

Figures

◀

▶

◀

▶

Back

Close

Full Screen / Esc

Printer-friendly Version

Interactive Discussion



Pyrocumulus and pyrocumulonimbus initiation and development

N. P. Lareau and
C. B. Clements

Title Page

Abstract

Introduction

Conclusions

References

Tables

Figures

◀

▶

◀

▶

Back

Close

Full Screen / Esc

Printer-friendly Version

Interactive Discussion

(Fig. 9f). In fact, a short time later the plume ceased to penetrate through the boundary layer top and the pyroCu subsequently dissipated (not shown). We hypothesize that the weakening updraft makes the plume more susceptible to the environmental wind shear, leading to increasing plume tilt with time. Also of note, the reversed flow aloft tends to sweep a portion of the plume back towards the lidar, which separates the upper plume from the convective column rising through the boundary layer. The role of wind shear as a limiting factor in plume development is further discussed in the thermodynamics section below.

3.2 Radar plume tops

Since definitive lidar detection of the plume tops was not possible, radar data is again used to estimate the maximum smoke injection depth. The Rocky Fire was within range of both the Sacramento (KDAX) and Beale Air Force Base (KBBX) NWS radars, and the data from both sites are in good agreement. As such, here we show only the results from KDAX echo tops product (Fig. 10).

The maximum radar echoes occur between 7500 and 8000 m, consistent with the lidar cloud detections during the first Rocky Fire pyroCu event. Relative to the fire perimeters, the local plume top maxima coincide with portions of the fire that expanded most rapidly on 30 July. Specifically, the first convective pulse corresponds to the expanding northwest flank, and the second to the southeast flank. The plume on the northeast flank was out of the lidar range, but appears to have attained similar plume heights.

3.3 Thermodynamic analysis

The Rocky Fire pyroCu development is interesting in that the thermodynamic environment theoretically supports much deeper convection than was observed. Using radiosonde data from ~ 10 km southwest of the fire (again after sunset), Fig. 11a shows that moist adiabatic ascent from the observed 4200 m cloud base would generate

Pyrocumulus and pyrocumulonimbus initiation and development

N. P. Lareau and
C. B. Clements

Title Page

Abstract

Introduction

Conclusions

References

Tables

Figures

◀

▶

◀

▶

Back

Close

Full Screen / Esc

Printer-friendly Version

Interactive Discussion



2035 J kg⁻¹ of CAPE and that the plume equilibrium level would be ~ 13 km, impinging on the tropopause. The radar data, lidar data, and visual observations all indicate, however, that the plumes ascended to no higher than ~ 8 km, corresponding to plume top temperature of $\sim -20^\circ\text{C}$. As such, these clouds are best classified as pyroCu, and never developed as deep pyroCb.

What then limits the growth? There appear to be two related limiting factors in the plume rise: (1) wind shear, and (2) entrainment of dry air into the plume. The lidar wind profiles, presented above in Figs. 8 and 9, indicate significant wind shear between the CBL and free troposphere. This wind shear is also apparent in the radiosonde wind profile, which shows a 180-degree wind shift at 2300 m. The flow below this level is from the west-northwest, whereas the flow above, and extending up to ~ 7 km, is from the east-southeast. The layer of southeasterly flow is associated with a surge of monsoonal moisture.

A second layer of significant wind shear at 7000 m separates the monsoon flow from southwesterly flow in the upper troposphere. This shear also coincides with a rapid decrease in dew point temperature, and thus relative humidity. It is notable then that the maximum echo tops occur only about 1 km above the upper shear layer. In fact, visual and photographic observations throughout the afternoon and early evening (not shown) clearly indicate this shear zone affected the pyroCu development, tending to sweep the upper portion of the cloud away from the updraft core. The detraining upper portions of the cloud subsequently developed ragged and wispy edges indicative of dry air entrainment as opposed to the crisp crenellations of growing cumulus congestus. In addition, when the full column is considered, the two shear layers combine to create a zigzag wind profile. This configuration is particularly detrimental to sustained upright convective columns, and presumably contributes to the limited plume heights observed in this case despite the substantive CAPE. This result is not surprising in that moist adiabatic ascent and CAPE are known to overestimate convective development and updraft strength due to the combined effects of entrainment, wind shear, and opposing pressure gradient perturbations (Markowski and Richardson, 2011).

Pyrocumulus and pyrocumulonimbus initiation and development

N. P. Lareau and
C. B. Clements

Title Page

Abstract

Introduction

Conclusions

References

Tables

Figures

◀

▶

◀

▶

Back

Close

Full Screen / Esc

Printer-friendly Version

Interactive Discussion



Despite the limited vertical development, these pyroCu observations provide additional support for the hypothesis that plume condensation levels exceed the ambient LCL. Following the same procedures described for the Bald Fire, the LCL for the MU parcel is 3503 m, and for the ML parcel is 3768 m (Fig. 11b). In contrast, the computed CCL of 4250 m is much closer to the lidar observed condensation level at ~ 4200 m. These results, like those from the Bald Fire, again suggest that the CCL is a useful parameter for estimating pyroCu/Cb convective initiation heights.

3.4 Fire radiative power and environmental moisture

Figure 12a shows the GOES-15 fire radiative power (FRP) in MW for the Rocky Fire on 29–30 July 2015. FRP is derived by differencing fire pixels from adjacent non-fire pixels using infrared radiance (Wooster, 2002) and has been shown to provide high fidelity representation of fire activity during California wildfires (Koltunov et al., 2012; Peterson et al., 2015). From these data it is clear that the diurnal cycle of fire intensity is similar during the first two days of the fire, with peak FRP values near 1500 MW each afternoon. What is notable, then, is that pyroCu were not observed on 29 July despite comparable fire intensity to 30 July when pyroCu were widespread.

To better understand this disparity, Fig. 12b shows a time series of the water vapor mixing ratio from a surface weather station near the Rocky Fire perimeter (data obtained from MesoWest, Horel et al., 2002), and Fig. 12c contrasts the 00:00 UTC soundings for two afternoons from the nearby Oakland, CA International Airport (KOAK). From these figures it is apparent that the onset of pyroCu on 30 July corresponds to the arrival of much higher humidity air, both at the surface and aloft. For example, the mixing ratio increases from 4.5 to 8 g kg⁻¹ while the relative humidity at 550 hPa jumps from 7 to 66 %. The corresponding change in the CCL is substantial, dropping from 5848 m a.m.s.l. on 29 July to 4267 m a.m.s.l. on the 30 July. Since the fire intensity remained constant during that time it is likely that the reduction in the CCL due to the influx of monsoon moisture was the driving factor in pyroCu formation. These observations further support the conclusions of Luderer et al. (2006, 2009) that envi-

Pyrocumulus and pyrocumulonimbus initiation and development

N. P. Lareau and
C. B. Clements

Title Page

Abstract

Introduction

Conclusions

References

Tables

Figures

◀

▶

◀

▶

Back

Close

Full Screen / Esc

Printer-friendly Version

Interactive Discussion

extend lofted debris affects buoyancy. Some potential avenues for obtaining these data include dropsondes from aircraft, surface and aircraft based radars, unmanned aerial vehicles, and dual-doppler lidar deployed during large-scale prescribed burn experiments where the fuel loading and extent of combustion is known or can be determined after the fact.

Author contributions. C. Clements conceived of the field project, N. Lareau and C. Clements conducted the field measurements, and N. Lareau led the data analysis and writing.

Acknowledgements. The lidar and radiosonde data are available upon request from the authors. All other data sources are publically available. This research is supported under grant AGS-1151930 from the National Science Foundation. Christopher C. Camacho contributed to the field observations during the Rocky Fire.

References

- American Meteorological Society: “Pyrocumulus”, Glossary of Meteorology, available at: <http://glossary.ametsoc.org/wiki/Pyrocumulus> (last access: October 2015), 2012a.
- American Meteorological Society: “Pyrocumulonimbus”, Glossary of Meteorology, available at: <http://glossary.ametsoc.org/wiki/Pyrocumulonimbus> (last access: October 2015), 2012b.
- Banta, R. M., Olivier, L. D., Holloway, E. T., Kropfli, R. A., Bartram, B. W., Cupp, R. E., and Post, M. J.: Smoke-column observations from two forest fires using Doppler lidar and Doppler radar, *J. Appl. Meteorol.*, 31, 1328–1349, doi:10.1175/1520-0450(1992)031<1328:SCOFTF>2.0.CO;2, 1992.
- Clements, C. B. and Oliphant, A. J.: The California State University mobile atmospheric profiling system: A facility for research and education in boundary layer meteorology, *B. Am. Meteorol. Soc.*, 95, 1713–1724, doi:10.1175/BAMS-D-13-00179.1, 2014.
- Cunningham, P. and Reeder, M. J.: Severe convective storms initiated by intense wildfires: Numerical simulations of pyro-convection and pyro-tornadogenesis, *Geophys. Res. Lett.*, 36, L12812, doi:10.1029/2009GL039262, 2009.
- Emanuel, K. A.: Atmospheric convection, Oxford University Press, New York, New York, USA, 580 pp., 1994.

Wooster, M. J.: Small-scale experimental testing of fire radiative energy for quantifying mass combusted in natural vegetation fires, *Geophys. Res. Lett.*, 29, 2027, doi:10.1029/2002GL015487, 2002.

Pyrocumulus and pyrocumulonimbus initiation and development

N. P. Lareau and
C. B. Clements

Title Page

Abstract

Introduction

Conclusions

References

Tables

Figures



Back

Close

Full Screen / Esc

Printer-friendly Version

Interactive Discussion



Pyrocumulus and pyrocumulonimbus initiation and development

N. P. Lareau and
C. B. Clements

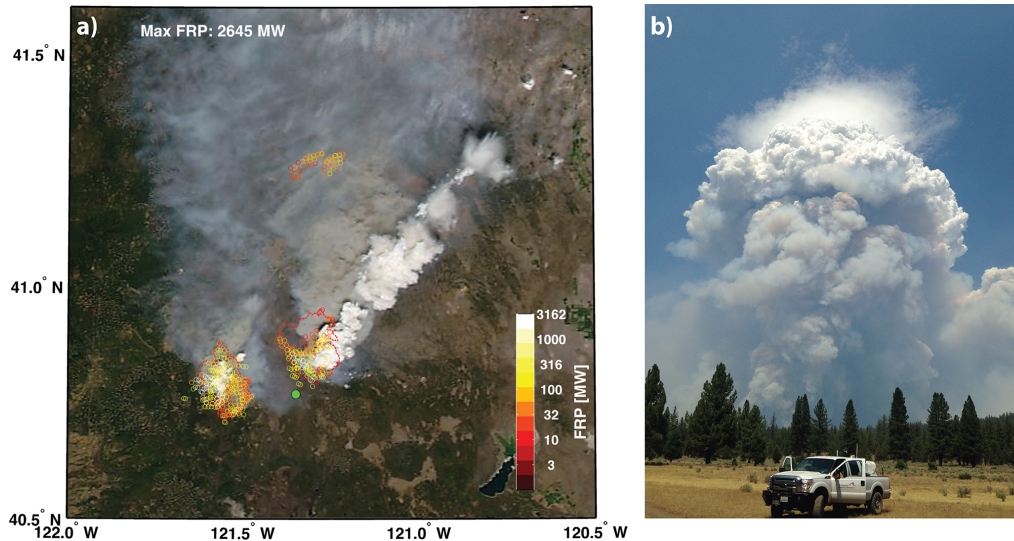


Figure 1. Overview of the Bald Fire. On 2 August 2014. **(a)** MODIS true color image at $\sim 14:30$ PDT overlaid with MODIS Fire Radiative Power (colored circles), and fire perimeters (dashed red lines). The maximum FRP is annotated and the truck location is shown as a green dot. **(b)** Photograph of the Bald Fire pyrocumulus at $\sim 14:20$ PDT showing the lidar vantage of the windward plume edge.

[Title Page](#)[Abstract](#)[Introduction](#)[Conclusions](#)[References](#)[Tables](#)[Figures](#)[◀](#)[▶](#)[◀](#)[▶](#)[Back](#)[Close](#)[Full Screen / Esc](#)[Printer-friendly Version](#)[Interactive Discussion](#)

Pyrocumulus and pyrocumulonimbus initiation and development

N. P. Lareau and
C. B. Clements

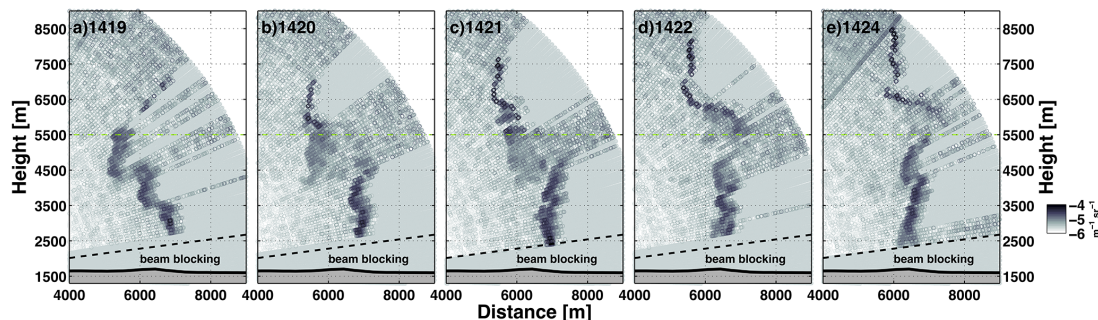


Figure 2. Lidar attenuated backscatter ($\text{m}^{-1} \text{sr}^{-1}$) sequence of the plume rise during the onset of a pyrocumulus on 2 August 2014. Flat gray shading shows where the lidar beam is attenuated. Times in PDT are shown next to the panel labels, and the light green line indicates the condensation level at 5500 m a.m.s.l.

[Title Page](#)[Abstract](#)[Introduction](#)[Conclusions](#)[References](#)[Tables](#)[Figures](#)[◀](#)[▶](#)[◀](#)[▶](#)[Back](#)[Close](#)[Full Screen / Esc](#)[Printer-friendly Version](#)[Interactive Discussion](#)

Pyrocumulus and pyrocumulonimbus initiation and development

N. P. Lareau and
C. B. Clements

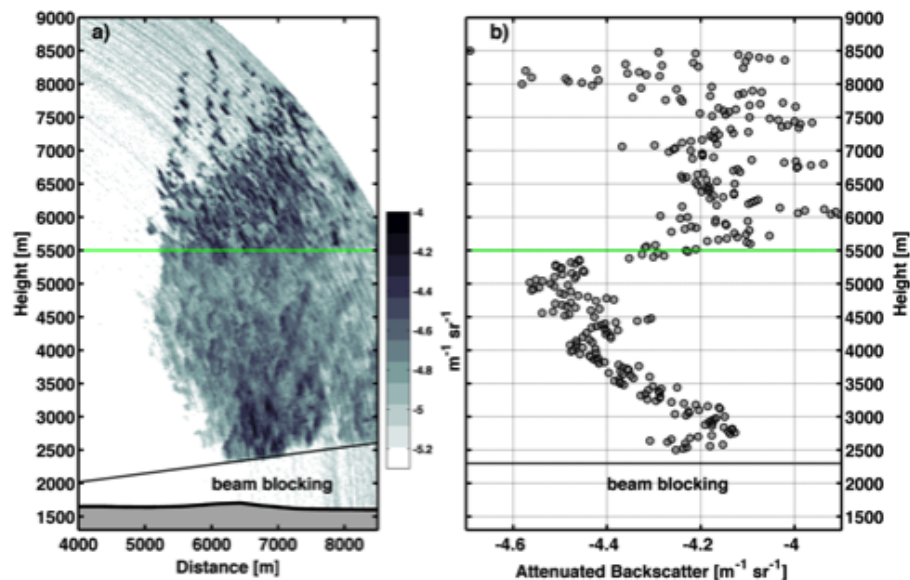


Figure 3. Aggregate of lidar plume scans between 14:00 and 15:30 PDT. **(a)** Maximum backscatter as a function of height and distance. **(b)** Maximum backscatter as a function of height only.

Pyrocumulus and pyrocumulonimbus initiation and development

N. P. Lareau and
C. B. Clements

Title Page

Abstract

Introduction

Conclusions

References

Tables

Figures

◀

▶

◀

▶

Back

Close

Full Screen / Esc

Printer-friendly Version

Interactive Discussion

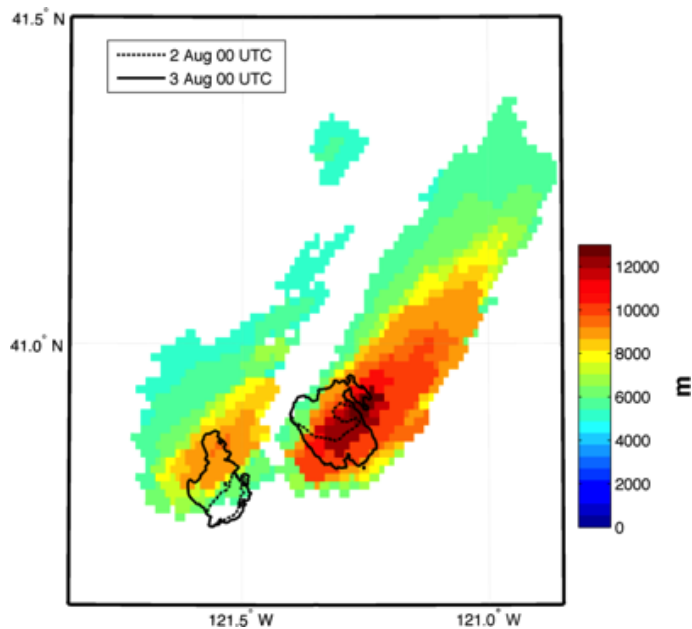


Figure 4. Radar derived echo tops for the Bald and Eiler Fires along with the evening fire perimeters.

Pyrocumulus and pyrocumulonimbus initiation and development

N. P. Lareau and
C. B. Clements

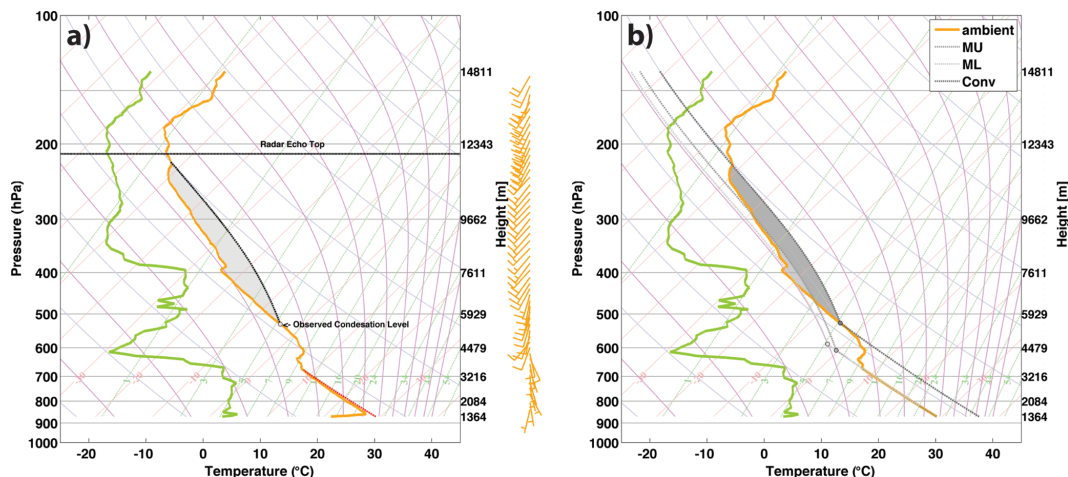


Figure 5. Skew-T Log-P diagrams showing radiosonde and parcel data during the Bald Fire Pyrocumulus event. **(a)** Observed temperature (orange) and dewpoint (green), modified CBL profile (dashed red), and observed condensation level, assumed moist adiabatic ascent (black dashed) with CAPE (grey shading). Also noted is the radar estimated echo tops. **(b)** Lifted parcel trajectories including the most unstable (MU), mixed-layer (ML), and convective parcels. The CAPE for each parcel is shaded and the condensation level for each parcel is denoted with a circle.

Pyrocumulus and pyrocumulonimbus initiation and development

N. P. Lareau and
C. B. Clements

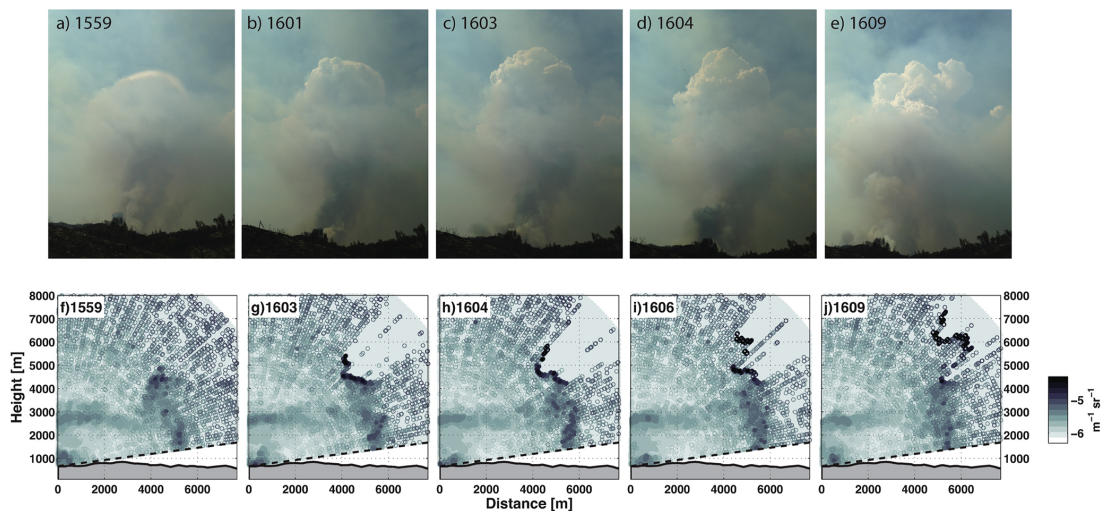


Figure 6. Pyrocumulus development during the Rocky Fire on 30 July 2015. **(a–e)** Photographs of the plume rise and pyroCu development. **(f–j)** Lidar backscatter showing the onset of condensation and subsequent cloud growth. All times are PDT.

Pyrocumulus and pyrocumulonimbus initiation and development

N. P. Lareau and
C. B. Clements

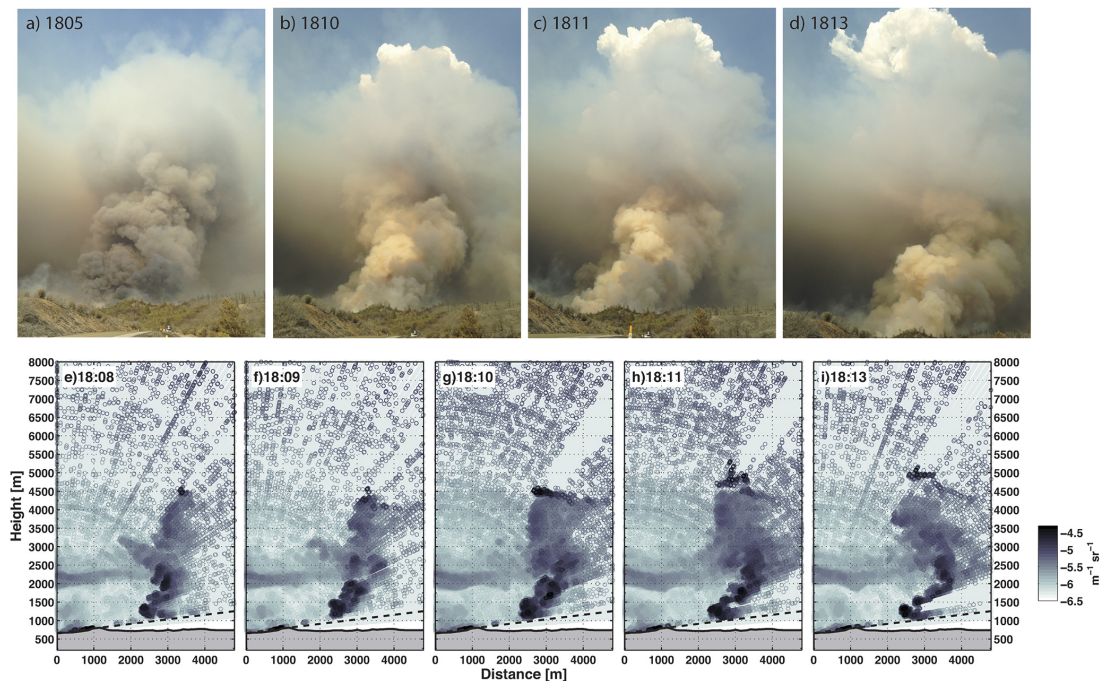


Figure 7. Second pyrocumulus development event during the Rocky Fire on 30 July 2015. **(a–d)** Photographs of the plume rise and pyroCu development. **(e–i)** Lidar backscatter showing the onset of condensation and subsequent cloud growth. All times are PDT.

[Title Page](#)
[Abstract](#)
[Introduction](#)
[Conclusions](#)
[References](#)
[Tables](#)
[Figures](#)
[Back](#)
[Close](#)
[Full Screen / Esc](#)
[Printer-friendly Version](#)
[Interactive Discussion](#)

Pyrocumulus and pyrocumulonimbus initiation and development

N. P. Lareau and
C. B. Clements

Title Page

Abstract

Introduction

Conclusions

References

Tables

Figures

◀

▶

◀

▶

Back

Close

Full Screen / Esc

Printer-friendly Version

Interactive Discussion

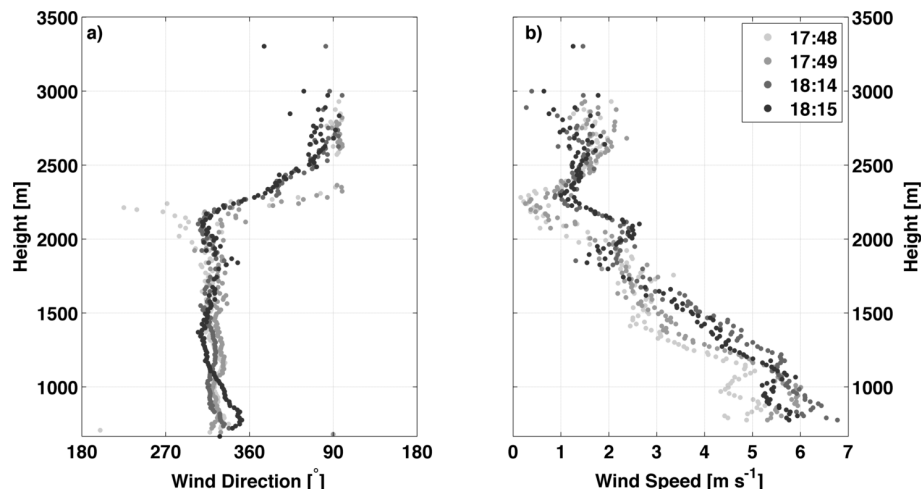


Figure 8. Lidar derived wind profiles during the second Rocky Fire pyrocumulus event. **(a)** Wind direction profiles, and **(b)** wind speed profiles. Gray shading corresponds to the time of the wind profile, which is shown in PDT in the legend.

Pyrocumulus and pyrocumulonimbus initiation and development

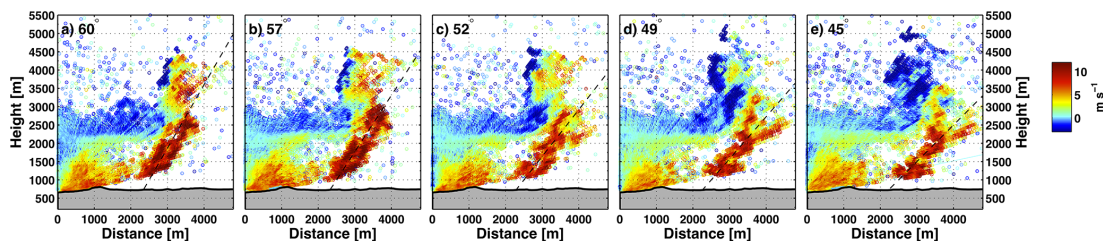
N. P. Lareau and
C. B. Clements

Figure 9. Lidar radial velocity during the second Rocky Fire plume rise sequence. Times are as in Fig. 7. Warm (cool) colors correspond to outbound (inbound) flow. The plume tilt angle is displayed adjacent to the panel label and the plume center line indicated as a black dashed line.

[Title Page](#)[Abstract](#)[Introduction](#)[Conclusions](#)[References](#)[Tables](#)[Figures](#)[⏪](#)[⏩](#)[◀](#)[▶](#)[Back](#)[Close](#)[Full Screen / Esc](#)[Printer-friendly Version](#)[Interactive Discussion](#)

Pyrocumulus and pyrocumulonimbus initiation and development

N. P. Lareau and
C. B. Clements

Title Page

Abstract

Introduction

Conclusions

References

Tables

Figures

◀

▶

◀

▶

Back

Close

Full Screen / Esc

Printer-friendly Version

Interactive Discussion

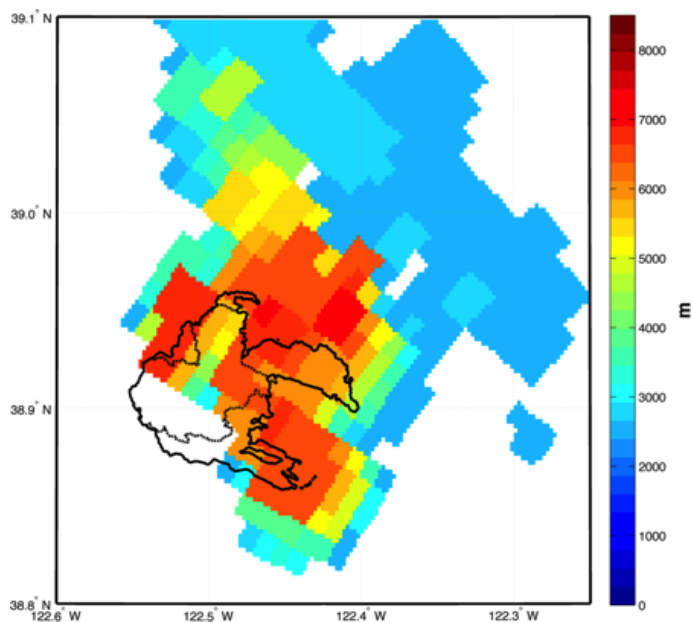


Figure 10. Radar derived echo tops for the Rocky Fire along with the evening fire perimeters.

Pyrocumulus and pyrocumulonimbus initiation and development

N. P. Lareau and
C. B. Clements

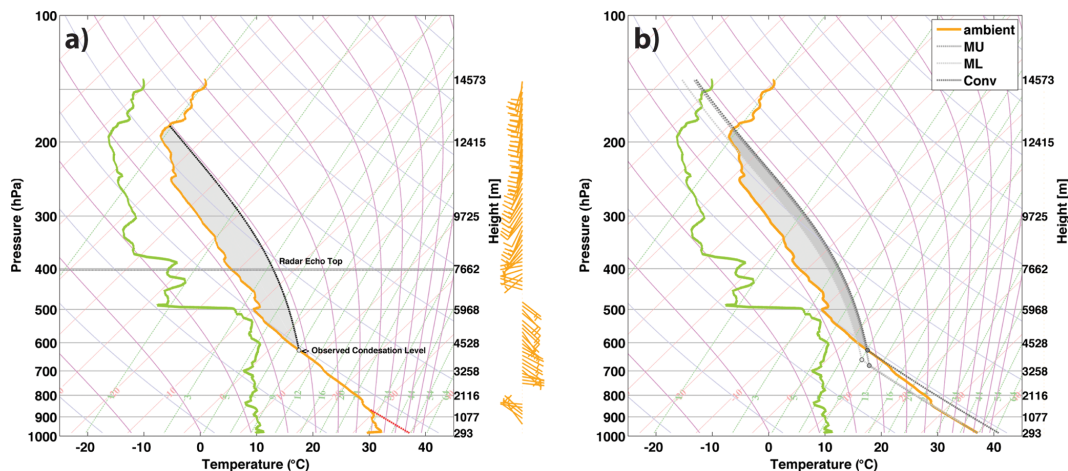


Figure 11. Skew-T Log-P diagrams showing radiosonde and parcel data during the Rocky Fire Pyrocumulus event. **(a)** Observed temperature (orange) and dewpoint (green), modified CBL profile (dashed red), and observed condensation level, assumed moist adiabatic ascent (black dashed) with CAPE (grey shading). Also noted is the radar estimated echo tops. **(b)** Lifted parcels including the most unstable (MU), mixed-layer (ML), and convective parcels. The CAPE for each parcel is shaded and the condensation level for each parcel is denoted with a circle.

Title Page

Abstract

Introduction

Conclusions

References

Tables

Figures

◀

▶

◀

▶

Back

Close

Full Screen / Esc

Printer-friendly Version

Interactive Discussion

Pyrocumulus and pyrocumulonimbus initiation and development

N. P. Lareau and
C. B. Clements

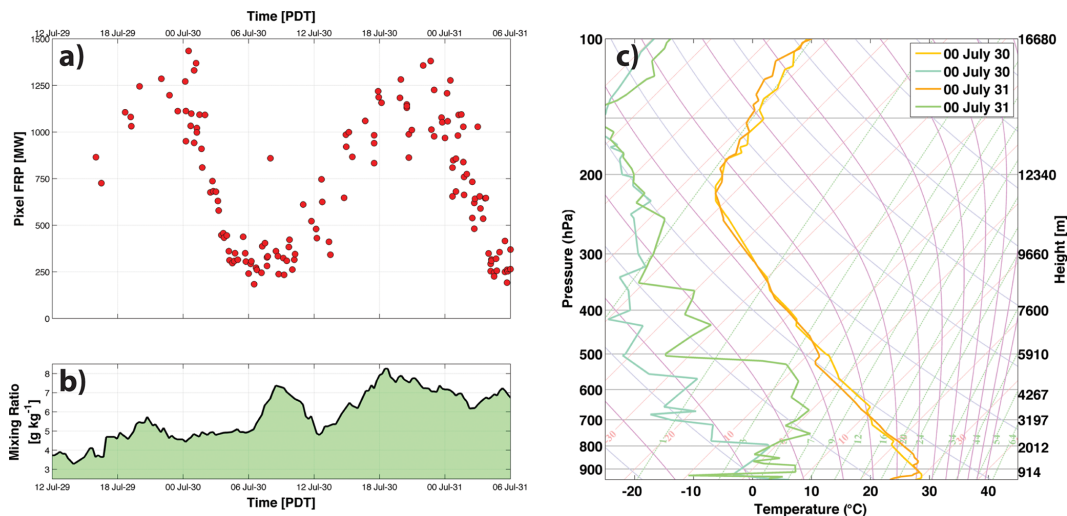


Figure 12. Overview of diurnal changes in fire intensity and environmental moisture between 29 and 30 July 2015. **(a)** GOES-15 Fire Radiative Power (FRP) in MW. **(b)** Surface water vapor mixing ratio, **(c)** KOAK soundings showing significant changes in mid-level moisture between 29 and 30 July.